Vibration Simulation of the Turbine Rotor System of an Underwater Vehicle Considering the Bearing Radial Clearance

Jing Liu, Lei Xue and Hengtai Ni

School of Marine Science and Technology, Northwestern Polytechnical University, Xi'an, 710072, P. R. China. Laboratory for Unmanned Underwater Vehicle, Northwestern Polytechnical University, Xi'an, 710072, P. R. China. E-mail: jliu@cqu.edu.cn

Wen Song and Yang Yang

The 705 Research Institute, China Shipbuilding Industry Corporation, Xi'an, 710075, P. R. China.

Guang Pan

School of Marine Science and Technology, Northwestern Polytechnical University, Xi'an, 710072, P. R. China. Laboratory for Unmanned Underwater Vehicle, Northwestern Polytechnical University, Xi'an, 710072, P. R. China.

(Received 18 May 2022; accepted 12 September 2022)

The turbine rotor system (TRS) is one important part of an underwater vehicle (UV). Its vibration and noise characteristics can greatly affect the performance and service life of the UV. To study the influence of radial clearance of supporting bearings on the vibrations of the whole TRS of the UV, a flexible dynamic model of the TRS is established by using the finite element and multi-body methods. Vibrations of the TRS from the rigid and flexible dynamic models under different bearing clearance conditions are analyzed. Note that the TRS with the flexible body model can obtain more accurate vibrations than the rigid one. The maximum vibration amplitude increases with the increment of bearing clearance. The bearing clearance of 5 μm to 20 μm is more reasonable for controlling the system vibration. The smaller clearance of supporting bearings of the TRS can cause more stable vibration responses. This paper can provide additional guidance for the accurate simulation analysis method of the TRSs of the UVs.

1. INTRODUCTION

The turbine rotor system (TRS) is an important part of the underwater vehicle (UV). Its vibration and noise characteristics can greatly affect the performance and service life of the UV.[1] The nonlinear contact deformations of the supporting bearing of the UV have great influence on the vibrations of system,[2] especially for the high operating speeds. Clearance is one of the important influence factors of bearing nonlinear characteristics, which must be produced by the manufacturing processing.[3] Therefore, it is important to study the influence of a turbine supporting bearing clearance on the vibrations of the TRS, which could help in controlling the vibrations of TRSs.

Many studies have been conducted on the rigid-flexible coupling modelling methods of the TRS, and vibrations of the rotor system caused by the clearance. Hu[4] proposed a modelling method consisting of a rub-impact rotor system and established a relationship between the fault deformation and the periodic signal based on the Fourier series. The fault characteristics of chaos and bifurcation were analyzed. Sun[5] established a turbine bearing-rotor system model, in which the bearing clearance and nonlinear stiffness factors were considered. Li et al.[6] established the transient response equation of a TRS. The dynamic stiffness of supporting bearing and damping of the TRS were considered. The equation was solved by a numerical integration. The vibrations of a rotor system under different speed conditions were analyzed. Song[7] simplified the model of a TRS based on the finite element (FE) method. By solving the vibration equation, this work analyzed the vibrations of the TRS under different acceleration modes.

Moreover, to understand the vibrations of rotor systems caused by the clearance of the bearing, many studies were conducted. Fredric and Ehrich[8] discovered the bi-stable type phenomenon. The rotor speed was near the critical speed. There was a significant difference in the amplitude of the Bode diagram. This work explained the phenomenon by establishing and solving an analytical model of the Jeffcott rotor. The results showed that the bi-stable type phenomenon was caused by the bearing clearance. Tiwari et al.[9] studied the balanced rigid rotor system supported by deep groove ball bearings. They used the numerical integration and harmonic balance methods to solve the equations. They also analyzed the influence of the bearing radial clearance on the rotor dynamics. Harsha et al.[10] established a mathematical model of a rotor system, in which the nonlinear factors such as the Hertzian contact force and radial clearance were considered. A new calculation method was adopted to analyze the influence of bearing clearance on the dynamics of the balanced rotor system. Li[11] established a single-disk rotor model that addresses the bearing clearance and internal damping caused by the axial sliding friction of rolling elements. Based on the elastohydrodynamic lubrication theory, the coefficient expression of external damping of bearing including the clearance was derived according to the

bearing loads. Sang et al.[12] established a one-dimensional clearance-collision-friction model. They studied the dynamics of a rotor supporting system under different assembly clearances. Song et al.[13] established a dynamic model of a cantilever rotor-bearing system considering the nonlinear Hertz contact force, radial clearance, and other factors. They analyzed the influences of the rotor speed and bearing clearance on the nonlinear dynamic characteristics of a rotor system. Li et al.[14] established the static model of a four-point contact ball bearing to analyze influence of the clearance on the load distribution of the bearing. Hu et al.[15] studied the optimization design problem of a bearing-rotor system. They improved the optimization model and solution algorithm considering the bearing clearance.

According to the previous analysis, there were many studies that were focused on vibrations of rotor systems. However, the previous models were single rotor system models. Based on the above literature review, there are few studies regarding the vibration analysis of TRSs with different bearing clearance conditions. Although there are few studies on vibration analysis of the TRS that consider the clearance of supporting bearings, they only used rigid dynamic models. Therefore, to explore the influence of the radial clearance of the bearing on vibrations of the TRS, this paper analyzes the differences of vibrations from the rigid and flexible dynamic models of a TRS under different speed conditions. Based on the flexible dynamic model, the vibrations of a rotor system under different clearance conditions are analyzed. This study can provide new methods for analyzing vibrations of the TRS.

2. DYNAMIC MODELING OF THE TRS OF THE UV

2.1. Rigid Body Model

2.1.1. Contact force model

Based on the Hertz theory, the relationship between the contact force F_i and contact strain δ_i of the ith steel ball can be expressed as:[16–18]

$$F_i = K_n \delta_i^{3/2} \quad (i = 1, 2, \cdots, Z); \tag{1}$$

$$K_n = \frac{K_d K_{oil}}{K_d + K_{oil}}; \tag{2}$$

$$K_d = \left(\frac{32}{9 n_\delta^3 \eta^2 \Sigma\rho} \right); \quad K_{oil} = \frac{dF_i}{dh_c}; \tag{3}$$

where K_n $(n = i, e)$ is the composite contact stiffness coefficient between the ball and two rings, which is composed of K_d and K_{oil}; K_d $(d = i, e)$ is the bearing contact stiffness coefficient without lubrication; K_{oil} is the oil film stiffness coefficient; n_δ is the coefficient related to the principal curvature difference function $F(\rho)$; η is the comprehensive elastic constant of two contact objects; and $\Sigma\rho$ is the principal curvature function of contact point. When the ball bearing is unloaded, there is the radial clearance u_r between the ball and rings. When the bearing is loaded, the center of inner ring offset; and the ball is contacted with the rings, which contributed to the elastic contact deformation. The total contact deformation δ_i between ith ball and two rings is given as:

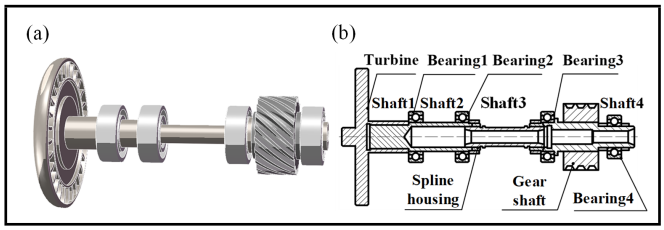

Figure 1. The geometric model of rotor system. (a) 3D entity diagram and (b) cross section of the TRS.

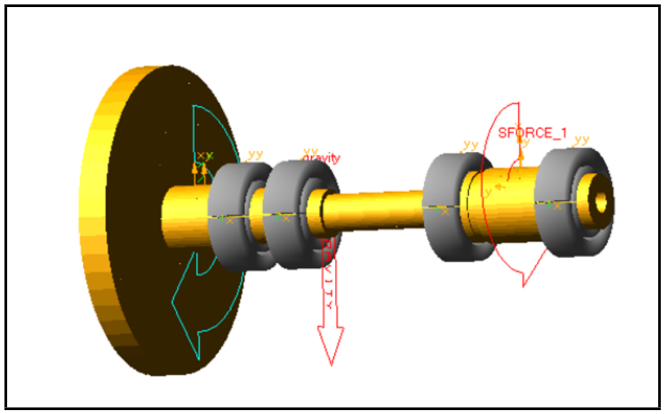

Figure 2. A multi-body dynamic model of the TRS.

$$\delta_i = (\delta_y \cos\Psi_i + \delta_x \sin\Psi_i) - \frac{1}{2} u_r; \tag{4}$$

where u_r is the initial radial clearance between the ball and rings; δ_x and δ_y are the offsets of geometric center points of inner ring along x and y directions; Ψ_i is the position angle of the ith ball. The radial load direction is the zero position angle.

The contact force between the ith ball and rings is as follows:[19,20]

$$F_j = K_n \left\{ \left[(\delta_y \cos\Psi_i + \delta_x \sin\Psi_i) - \frac{1}{2} u_r \right] H_i \right\}^{1.5}; \tag{5}$$

where H_i is the contact force judgement function; when the ball and ring are in contact, $H_i = 1$; when the ball does not contact with the ring, $H_i = 0$.

2.1.2. A multi-body dynamic model

The high-speed rotor system of turbine consists of one turbine disc, one hollow shaft, one spline sleeve, one gear shaft, and four deep groove ball bearings. The geometric model of rotor system is shown in Fig. 1.

The multi-body dynamic model is developed in the commercial software ADAMS. Due to the limitations of commercial software, the influence of the bearing cage on the vibrations of the rotor system is not studied in this paper. To simulate actual working conditions, it is necessary to drive and impose constraints on the model. A rotary drive is set between the turbine shaft and ground. The drive is expressed by the STEP function. A torque constraint is applied at the end of the model to stabilize the vibration of the rotor system. The multi-body dynamic model of the TRS is shown in Fig. 2.

2.2. A Rigid-Flexible Coupling Model

2.2.1. Theoretical algorithm

When the rotating speed of the TRS is a higher one, the influence of its deformation on the vibrations cannot be ignored. Thus, a rigid-flexible coupling dynamic model must be established. The rotor system has three main components, such as, a rotating shaft, additional rotating components and a supporting unit. In this model, in order to facilitate the study of vibrations of a rotor system, only the rotating shaft is a flexible one. The shaft is considered a shaft segment with a deformation capacity and mass uniformity. The additional rotating components are considered rigid discs, which have the same mass and rotational inertia as the additional rotational components such as turbines and gears. The supporting units are the bearings, which are precision parts. The size of each part of the bearing has a significant effect on vibrations of the bearing.

An infinite number of degrees of freedom of the rotating shaft is expressed by the axis node, which is realized as discretization. The elastic deformation of a node element is obtained by the linear superposition, which is as follows:[21]

$$[u] = \Sigma a_i [\Phi]_i; \tag{6}$$

where $[u]$ is the displacement vector of each node; α_i is the modal factor; $[\Phi]_i$ is the modal of element; x, y and z are the generalized displacements of node; θ_x, θ_y and θ_z are the rotation angles of node relative to the axis.

When the flexibility of a shaft is considered, the position of each node in the shaft is constantly changing. The local reference coordinate system cannot accurately describe the position of each node. We need to describe the position of each node by establishing an elastic coordinate system. The position is represented by the Cartesian coordinates x, y and z of nodes. The orientation is represented by the section torsion angles θ_x, θ_y and θ_z. The displacement vector is given as:[22]

$$[u] = [x \quad y \quad z \quad \theta_x \quad \theta_y \quad \theta_z]. \tag{7}$$

For the flexibile shaft, we need to consider the effect of stiffness. The modal coordinates are supposed as:

$$k = \{k_1, k_2, \cdots, k_M\}; \ (M \text{ is the modal number}). \tag{8}$$

The generalized coordinates of nodes are given as:

$$[u] = [x \quad y \quad z \quad \theta_x \quad \theta_y \quad \theta_z \quad k_j]^T; \tag{9}$$

where $j = 1, 2..., p$ and p represents modal order. The location vector of ith node is expressed as:

$$u_i = x + A(d_i + m_i k); \tag{10}$$

where A is the transformation matrix of inertial reference system; d_i represents the initial location of ith node; and m_i is the modal submatrix of ith node.

We can get the differential equations of motion of flexible axial element, which is given as:

$$M\ddot{u}_i + C\dot{u}_i + Ku_i = F; \tag{11}$$

where M is the mass matrix; C is the damping matrix; K is the stiffness matrix; F is the external load force; $\ddot{u}, \dot{u}, u$ and u are the vibration acceleration vector, vibration velocity vector and vibration displacement vector of ith node in the rotor system.

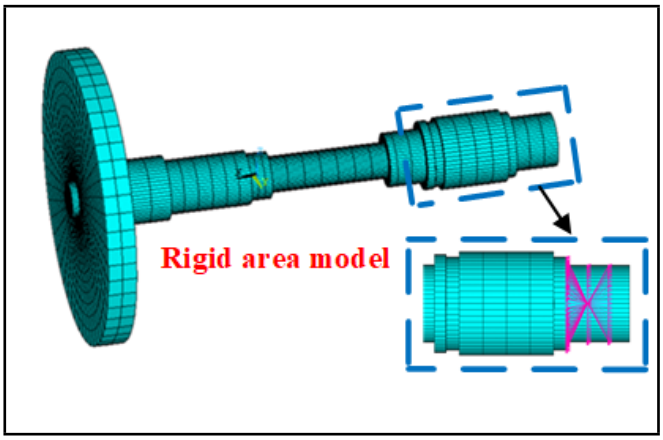

Figure 3. The FE model of the TRS.

2.2.2. A rigid-flexible coupling model

Here, the modal linear superposition is used to express its elastic deformation. It can realize the flexibility of the turbine shaft. The modal information file of turbine shaft will be obtained. The meshing of the FE model of the TRS is based on the hexahedron dominant principle. The mesh size is set to be 3 mm. The number of elements and notes of the FE model of the TRS are 10476 and 33488, respectively. The mesh divided is shown in Fig. 3. A modal information file is produced based on the software, which is used to establish the rigid part of model. The rigid area in the FE model is shown in Fig. 3. The mark points are setted as in the rigid area. In the rigid-flexible coupling dynamic model, the driving and constraints are applied as those in Fig. 2.

3. VIBRATION ANALYSIS OF THE TRS

3.1. Comparisons of Rigid and Flexible Models

Here, five-speed conditions of 6000 r/min, 18000 r/min, 30000 r/min, 48000 r/min, and 60000 r/min are used to study the vibrations from flexible models of the TRS, where the bearing clearance is 5 μm. The differences between the vibrations of rigid and flexible models of the TRS are analyzed.

The rotational speed is 6000 r/min. The comparative analyses of vibrations of rigid and flexible models are plotted in Fig. 4. The spectra show that the differences between the spectra of rigid and flexible models are small. The spectrum in the y direction has only one working frequency component (f_s). The spectrum in the z direction is dominated by f_s. The amplitudes of rigid and flexible models are 0.483 μm and 0.456 μm, respectively. The difference is 0.027 μm, which is so small. Moreover, the amplitude of peaks at $2f_s$ and $3f_s$ are small.

The rotational speed is 18000 r/min. The comparative analyses of vibrations of rigid and flexible models are plotted in Fig. 5. The spectra show that the differences between the spectra of rigid and flexible models are small and almost coincides. The vibration spectrum in the y direction has two frequency components. One peak is f_s. The amplitudes of rigid and flexible models are 0.802 μm and 0.792 μm, respectively. Their difference is 0.01 μm. Another peak is $2f_s$, which is obvious. The amplitudes of rigid and flexible models are 0.218 μm and 0.207 μm, respectively. Their difference is 0.011 μm. The frequency component in the z direction is the same as that in

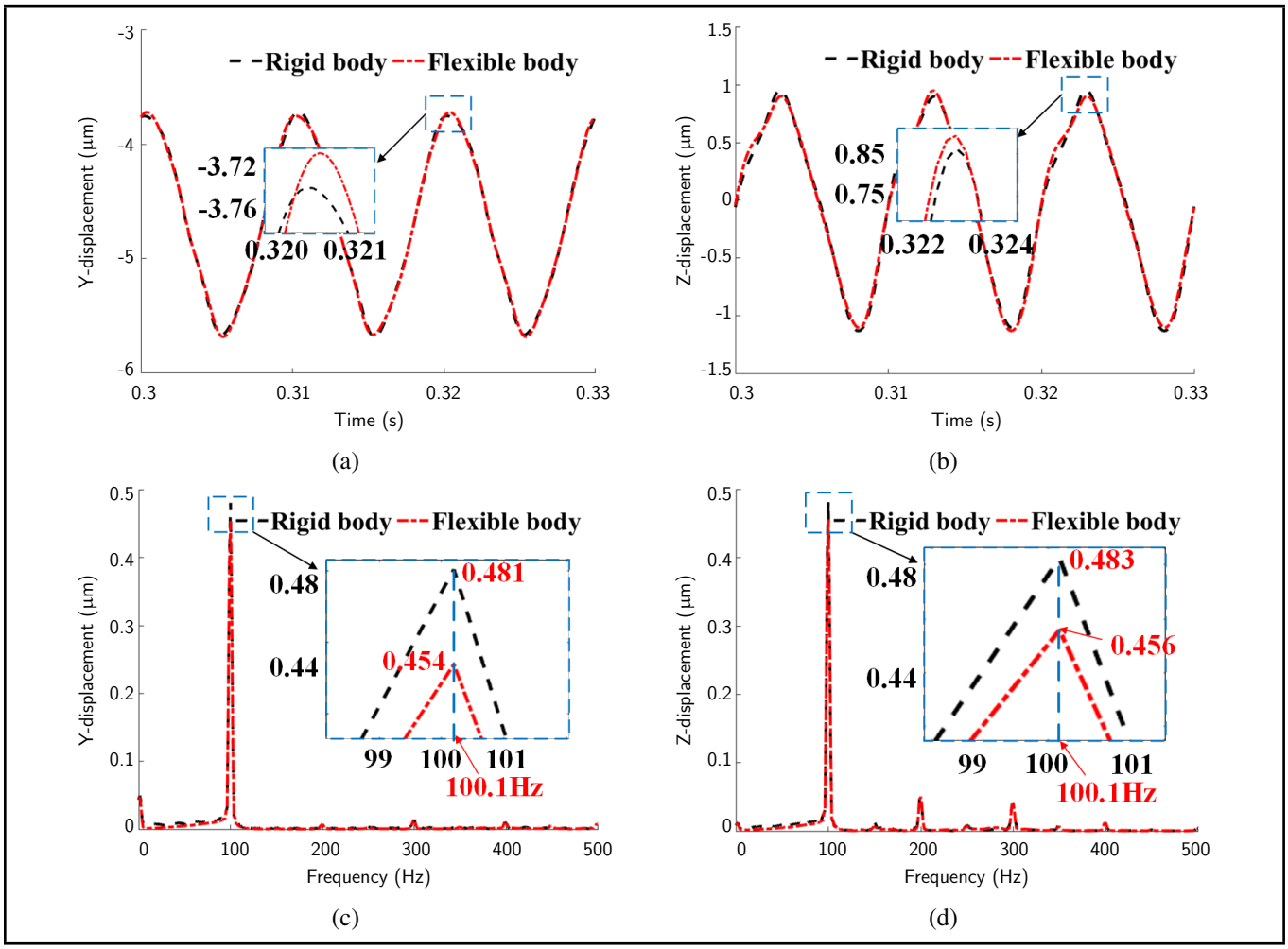

Figure 4. Comparison of vibrations of rigid and flexible models with a rotational speed of 6000 r/min. (a) Displacements in the y direction, (b) displacements in the z direction, (c) spectra of (a), and (d) spectra of (b).

the y direction. One is f_s and another is $2f_s$, which is weak. The amplitudes of rigid and flexible models are 0.728 μm and 0.725 μm, respectively. Their difference is 0.003 μm, which is quite small.

The rotational speed is 30000 r/min. The comparative analyses of vibrations of rigid and flexible models are plotted in Fig. 6. The spectra show that, in the y direction, the spectra of rigid and flexible models are quite different. The main frequencies are both f_s. But $1/2f_s$ of the flexible model is more obvious. The amplitude is 0.529 μm. The amplitude of peak at $1/2f_s$ of the rigid model is smaller. The amplitude is 0.529 μm. The frequency components in the z direction are different from those in the y direction. The differences in the spectra of rigid and flexible models are small. The main frequency is $1/2f_s$. f_s is more obvious, but the high frequencies are small.

The rotational speed is 48000 r/min. The comparative analyses of vibrations of rigid and flexible models are plotted in Fig. 7. The spectra show that the differences between the spectra of rigid and flexible models are small and almost coincides. The main frequency in the y direction is f_s. The amplitudes of rigid and flexible models are 0.674 μm and 1.016 μm, respectively. The differences is 0.011 μm, which is very small. There are many low-frequency components. The frequency components in the z direction are the same as those in the y direction. The main frequency is f_s. There are many low-frequency components.

The rotational speed is 60000 r/min. The comparative analysis of vibrations of rigid and flexible models is shown in Fig. 8. The spectra of rigid and flexible models are quite different. In the y direction, the main frequency of the flexible model is 402.8 Hz. f_s is obvious; and its amplitude is 1.084 μm. The main frequency of the rigid model is f_s; and it amplitude is 0.575 μm. The number of frequency components is small. The frequency components in the z direction are similar to that in the y direction. The main frequency of the flexible model is 402.8 Hz. f_s and is obvious; and its amplitude is 1.086 μm. The main frequency of the rigid model is f_s; and its amplitude is 0.504 μm. The number of frequency components is small.

Table 1. Amplitude comparison of rigid and flexible models in the y and z directions.

Rotational speed (r/min)	y directions (μm)			z directions (μm)		
	Rigid	Flexible	Difference	Rigid	Flexible	Difference
6000	0.48	0.49	0.01	1.00	1.05	0.05
18000	0.88	0.91	0.03	1.51	1.58	0.07
30000	1.80	2.51	0.71	3.53	4.24	0.71
48000	1.79	2.73	0.94	2.76	3.49	0.73
60000	1.10	7.95	6.85	1.02	8.37	7.35

The relative differences in amplitude of the model in y and z directions at different speeds are plotted in Table. 1. At the speeds of 6000 r/min and 18000 r/min, the amplitude differences between rigid and flexible models of the TRS are 0.01 μm and 0.03 μm in the y direction; The amplitude differences in the z direction are 0.05 μm and 0.07 μm. The differences are very small; and the curve almost overlap. There-

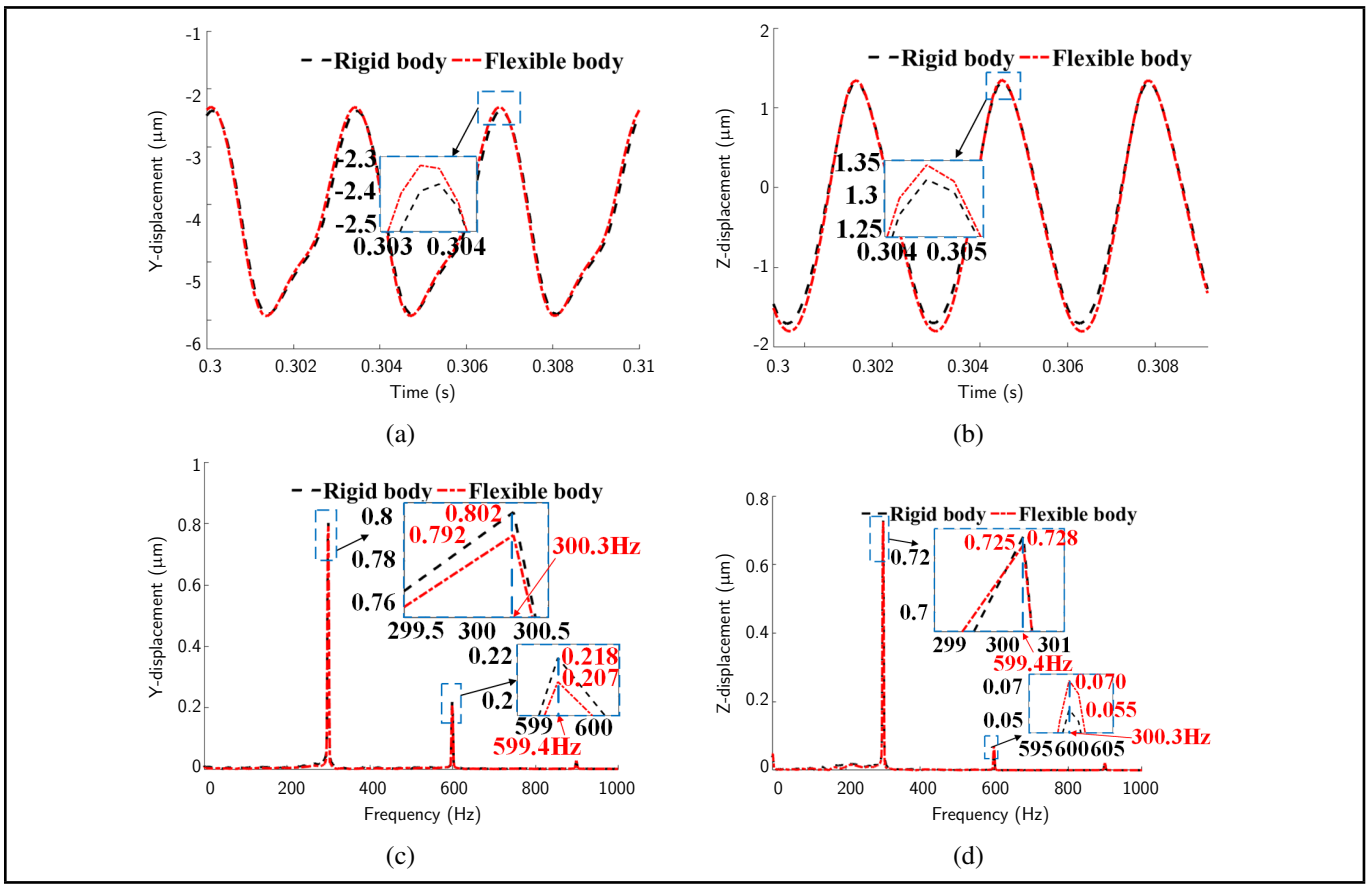

Figure 5. Comparison of vibrations of rigid and flexible models with a rotational speed of 18000 r/min. (a) Displacements in the y direction, (b) displacements in the z direction, (c) spectra in the y direction, and (d) spectra in the z direction.

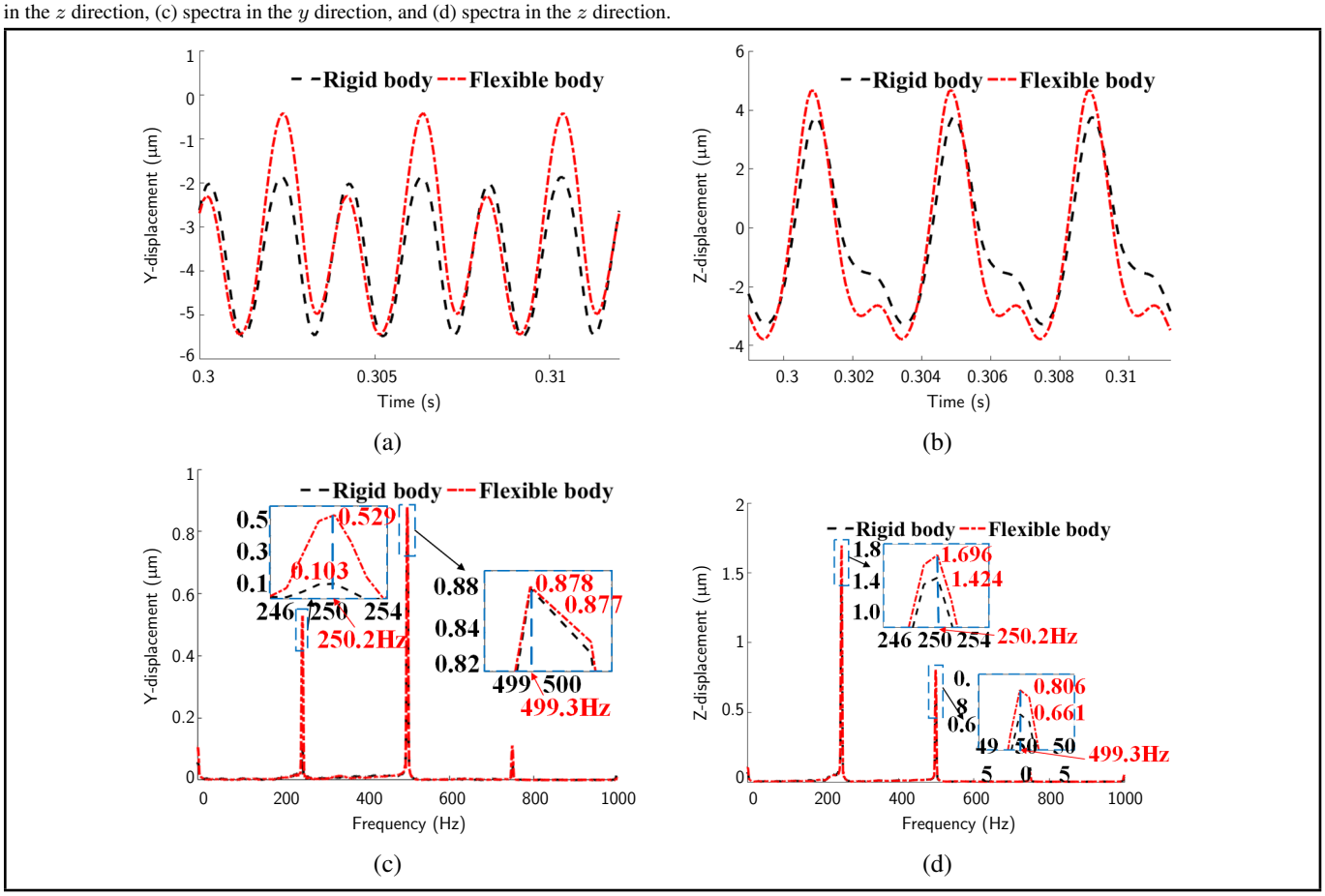

Figure 6. Comparison of vibrations of rigid and flexible models with a rotational speed of 30000 r/min. (a) Displacements in the y direction, (b) displacements in the z direction, (c) spectra in the y direction, and (d) spectra in the z direction.

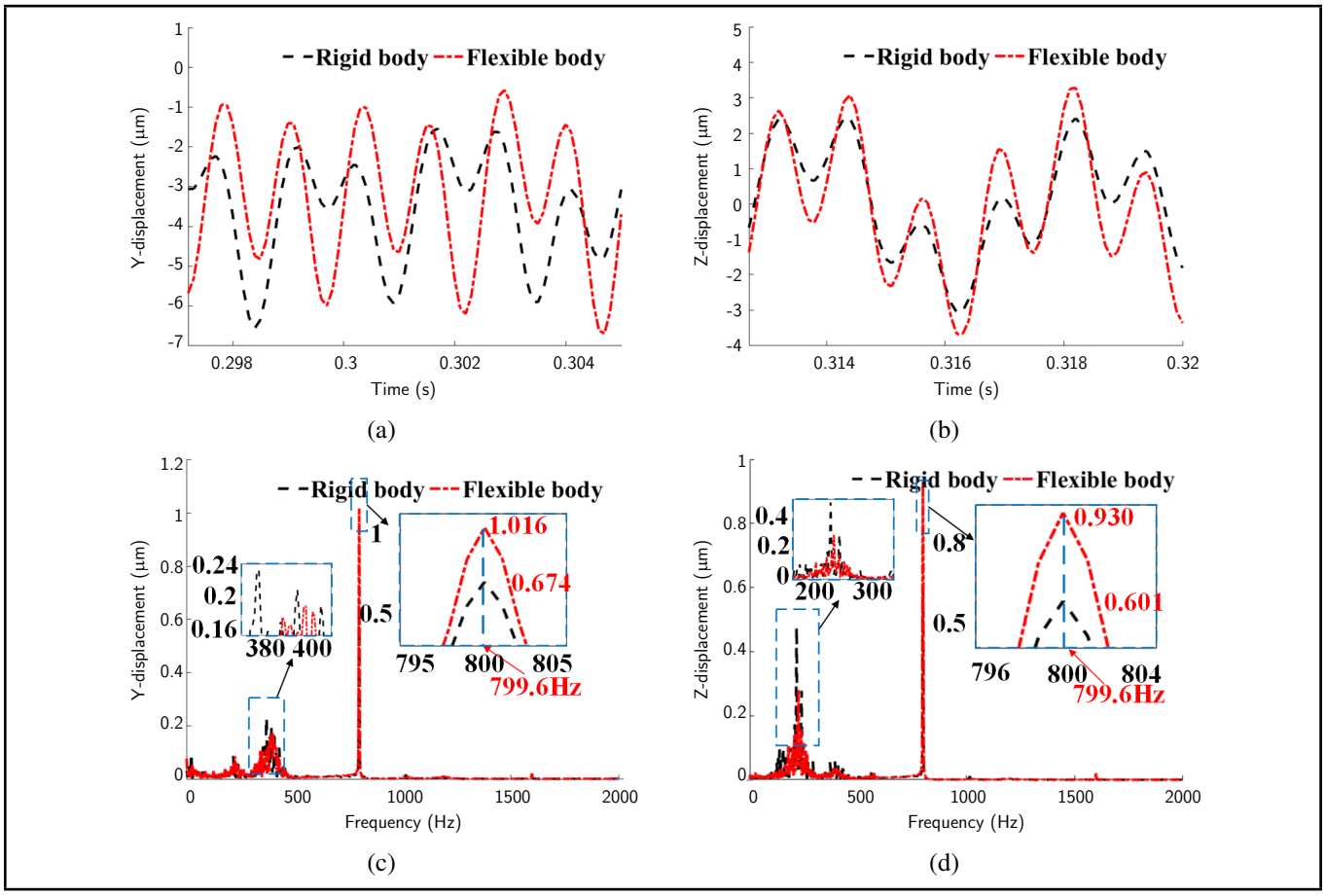

Figure 7. Comparison of vibrations of rigid and flexible models with a rotational speed of 48000 r/min. (a) Displacements in the y direction, (b) displacements in the z direction, (c) spectra of (a), and (d) spectra of (b).

fore, at low speeds, the vibrations of rigid and flexible models are relatively small; The amplitude differences between the rigid and flexible models of the TRS at the high speeds of 30000 r/min and 48000 r/min in the y direction is 0.71 μm and 0.94 μm; The amplitude differences in the z direction are 0.71 μm and 0.73 μm. There is a difference; and the difference can not be neglected. At the speed of 60000 r/min, the deformation of the flexible model increases, which leads to the amplitude increasing greatly. In the y direction, the maximum amplitude difference is 6.85 μm; In the z direction, the amplitude difference is 7.35 μm. In the case of low speed, the main frequencies in the y and z directions are f_s, the component is single. The amplitude of the rigid model is larger than that of the flexible model. When the rotation speed is gradually increased, the spectra in y and z directions will appear $1/2f_s$, and with complex low-frequency components. The amplitude of the flexible model will be larger than that of the rigid model under the same frequency component. The flexible model will also have frequency components that are not available in rigid ones. The deformations of the bearing and shaft will contribute to the rotor system imbalance including the mass imbalance, force imbalance, and dynamic imbalance, which may generate the frequency components that are not available in rigid ones. In the engineering practice, the rotating speed of the TRS of the UV is so high that the deformation of turbine shaft cannot be ignored. Therefore, the TRS with a flexible turbine shaft can better reflect the vibrations of rotor systems in actual working conditions.

3.2. Influence of the Clearance on the Vibrations of the TRS

Taking in account of the influence of the bearing clearance on the vibrations of the TRS, the working speed of the TRS is defined as 60000 r/min. The clearance conditions are 10 μm, 15 μm, 20 μm, 25 μm and 30 μm. The differences between the amplitude time-domain displacements and spectra of the flexible model of the TRS in the y and z directions under different clearance conditions are studied. The time-domain vibrations and their spectra from the flexible model under different clearance conditions are plotted in Fig. 10. In Figs. 10(a) and (b), when the bearing clearance are 5 μm, 10 μm, 15 μm, 20 μm, and 30 μm, the maximum amplitudes of the TRS in the y direction are 17.33 μm, 18.45 μm, 20.38 μm, 23.32 μm, and 31.17 μm. The maximum amplitudes in the z direction are 4.17 μm, 17.00 μm, 19.55 μm, 21.66 μm, and 27.70 μm. When the clearance gradually increases, the maximum vibration amplitude of the TRS also gradually increases. When the clearance is less than or equal to 20 μm, the maximum amplitude differences between the clearances in the y and z directions are 2.94 μm and 2.11 μm. The amplitude changes slightly. When the clearance is greater than 20 μm, the maximum amplitude differences among the clearance cases that are setted in the y and z directions are 7.85 μm and 6.04 μm. The amplitude increases significantly. Based on the previous research, an optimization scheme for supporting bearing clearance of the TRS is proposed. It is recommended that the clearance of the supporting bearing of the TRS should be controlled from 5 to 20 μm to reduce vibration levels and fatigue damage.

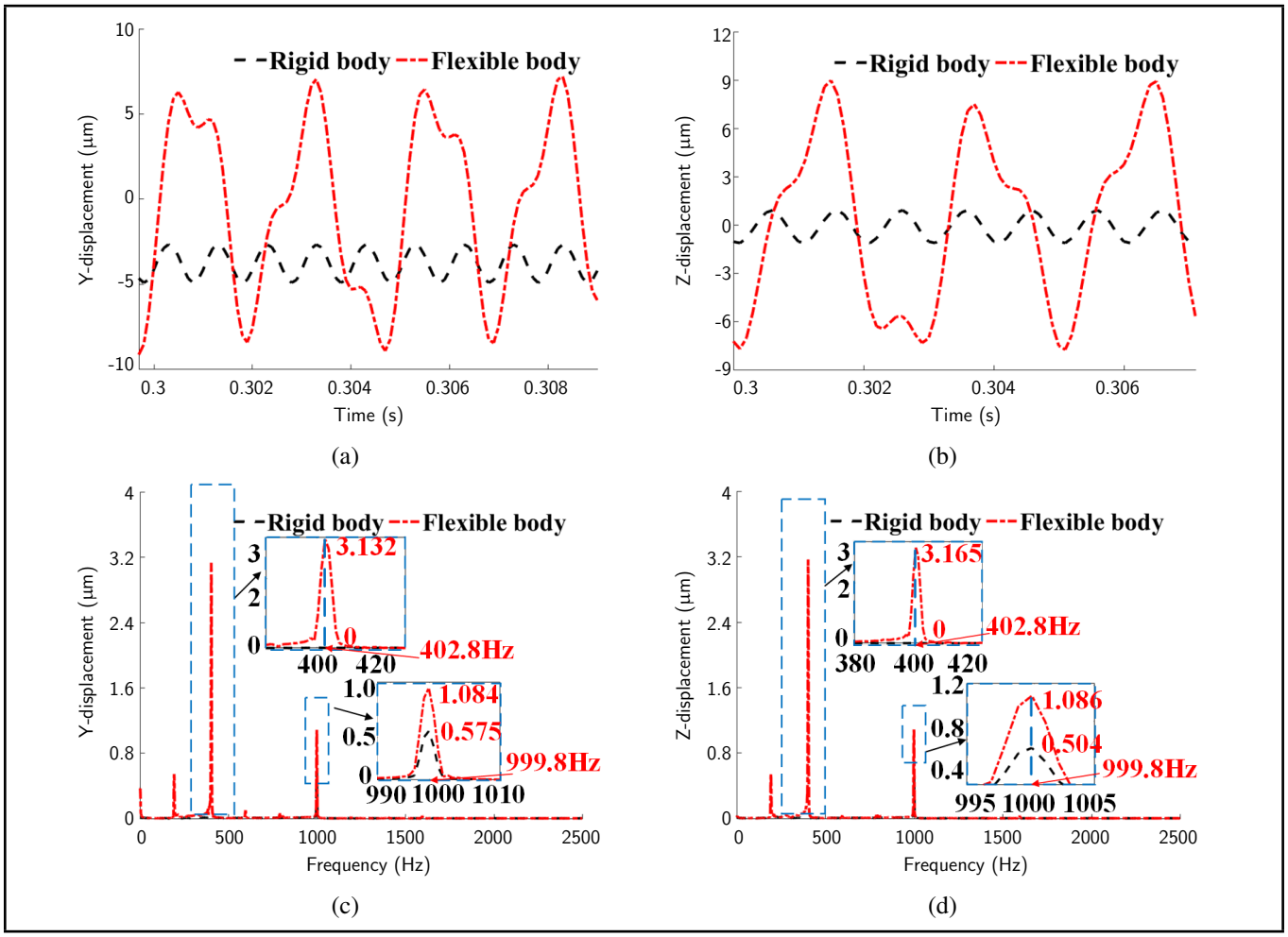

Figure 8. Comparison of vibrations of rigid and flexible models with a rotational speed of 60000 r/min. (a) Displacements in the y direction, (b) displacements in the z direction, (c) spectra in the y direction, and (d) spectra in the z direction.

In Figs. 10(c) and (d), when the bearing clearance are 5 μm, 10 μm, 15 μm, 20 μm, and 30 μm respectively, the RMS values of amplitude of the TRS in the y direction are 9.95 and 11.99, 14.06, 16.50 and 21.40, respectively. The RMS values of amplitude in the z direction are 4.76, 10.17, 12.65, 14.66, and 18.76, respectively. The RMS values of amplitude increase with the increment of the bearing clearance. The smaller clearance of supporting bearings of the TRS can cause more stable vibrations of the rotor system. The spectra are plotted in Figs. 10(e) and (f). Figure 10(e) gives the spectra of the TRS in the y direction. The peaks at $1/2f_s$ and its main frequency are observed. The amplitude at f_s is small. In the low-frequency components range, the frequencies corresponding to the bearing clearance of 5 μm, 10 μm, 15 μm, 20 μm and 30 μm in the y direction are 544.4 Hz, 537.1 Hz, 528.6 Hz, 529.8 Hz, and 521.1 Hz, respectively. Figure 10(f) gives the spectra of the TRS in the z direction. It can be seen that it is similar to the frequency distribution in the y direction. There is $1/2f_s$; and its main frequency is $1/2f_s$. The amplitude at f_s is weak. The corresponding frequencies in the z direction are 402.8 Hz, 490.7 Hz, 484.6 Hz, 472.4 Hz, and 456.5 Hz. In Fig. 10(g), the bearing clearances are 5 μm, 10 μm, 15 μm, 20 μm, and 30 μm from the left to right sides. The axis track appears as multiple overlapping and stable circles, and the radius of the circle increases with the increased bearing clearances. The smaller clearance of supporting bearings can lead to a more stable axis rotation.

4. MODAL VALIDATION

To verify the accuracy of the proposed flexible body model of the TRS, the critical speed of the TRS from the proposed FE method is compared with that from the experimental results given in References.[23] The intersection of the straight line (ω=Ω) and the curve in Fig. 11 are the critical speed corresponding to the vortex. There is a positive whirl curve in Fig. 11, which does not intersect the straight line (ω=Ω). The reason is that when the turbine disk is whirling in the forward direction, the stiffness of the turbine shaft increases under the action of the gyroscopic moment. Therefore, as the rotation angular velocity increases, the forward whirl frequency also increases sharply, which can cause the intersection not being observed. On the contrary, the stiffness of the turbine shaft decreases, which contributes to the intersection points. According to Campbell diagrams in Fig. 11, the first and second critical speeds are 4116.5 rad/s and 15567 rad/s. The first critical speed from the experiment in References[23] is 4297 rad/s. The difference of the first crictial speed from the simulation and experiment is 3.88%, which can give some validation for the proposed flexible model. The difference between the simulation and experiment maybe caused by the supported stiffness of rotor system. The bearing outer ring of the model is considered as a fixed part, but there is a small deformation of the bearing outer ring in an actual working condition, which has the influence on the support stiffness of the rotor system.

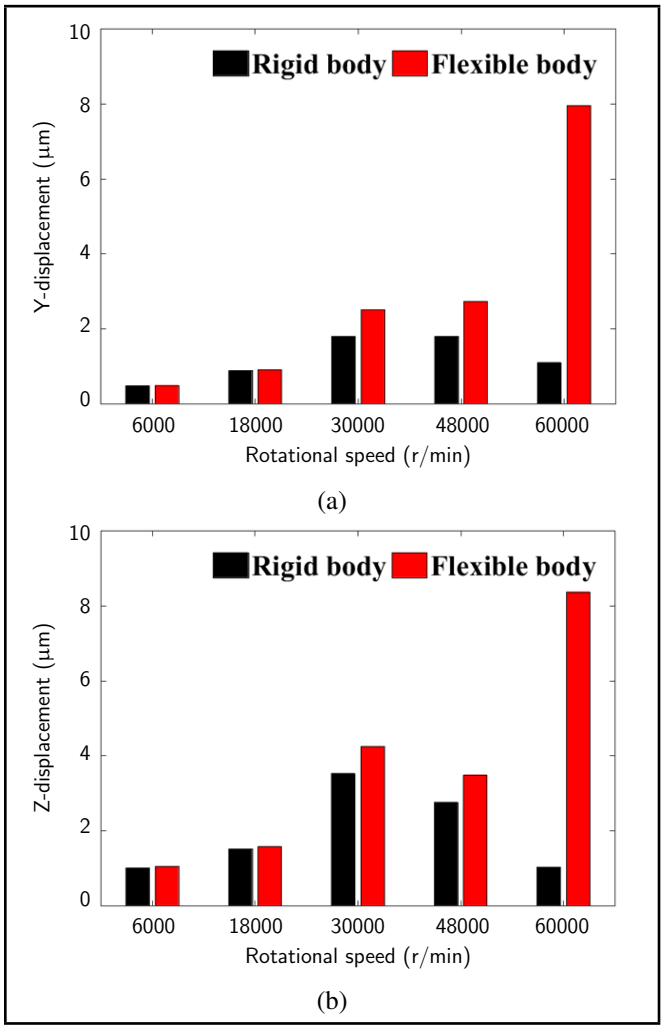

Figure 9. Displacement comparisons of rigid and flexible models in (a) y and (b) z directions.

5. CONCLUSIONS

This paper establishes the rigid and flexible models of the TRS of the UV in order to study the influence of the bearing radial clearance on the vibrations of the TRS. Some following conclusions can be drawn:

(1) At the speed conditions of 6000 r/min and 18000 r/min, the impact of the rigid and flexible turbine shaft on the vibrations of the TRS was very small. The maximum amplitude difference was 0.07 μm. The vibration amplitude and curve waveform were similar to each other, and the frequency components of rigid and flexible turbine shafts in the y and z directions were the same. The main frequency was f_s and the frequency component was single. At the speed conditions of 30000 r/min, 48000 r/min, and 60000 r/min, the effects of the rigid and flexible turbine shaft on the vibrations of the TRS was quite different. The maximum amplitude difference was 0.94 μm. The frequency components of rigid and flexible turbine shafts in the y and z directions was different. There was $1/2f_s$ and complex low-frequency components in the y and z directions. the TRS with the flexible turbine shaft obtained more accurate vibrations than the rigid one.

(2) The maximum displacement and RMS of amplitudes in the y and z directions of the TRS of the UV increased with increased clearance. They increased sharply after the clearance conditions of 20 μm. Therefore, the clearance of supporting bearing of the TRS of the UV should be controlled from 5 to 20 μm.

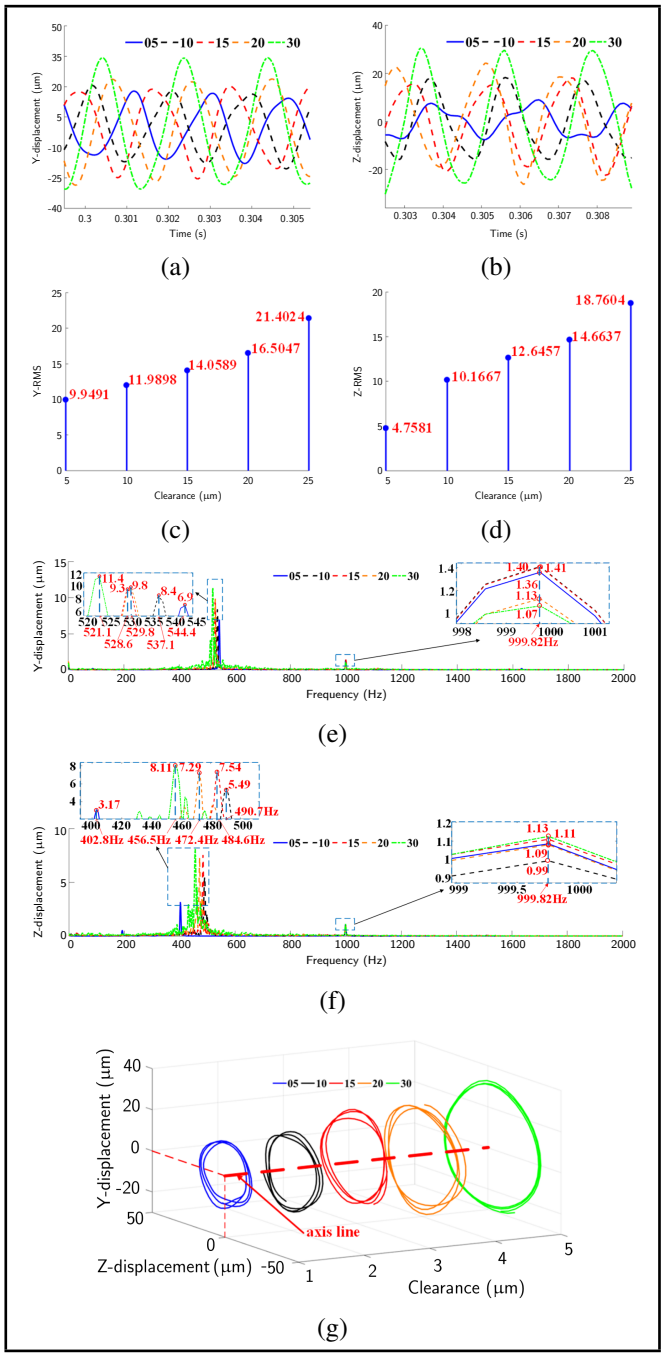

Figure 10. Time-domain vibrations and their spectra from flexible model under different clearance conditions. (a) Displacements in the y direction, (b) displacements in the z direction, (c) RMS value of displacements in the y direction, (d) RMS value of displacements in the z direction, (e) spectra in the y direction, (f) spectra in the z direction, and (g) axis track response.

(3) At the clearance conditions of 5 μm, 10 μm, 15 μm, 20 μm, and 30 μm, the frequency distributions of vibrations in the y and z directions was similar. There was $1/2f_s$; and the main frequency was $1/2f_s$. The amplitude at f_s was small.

(4) The axis track appeared as multiple overlapping and stable circles, and the circular area increased with increased clearance. The smaller clearance of the supporting bearings can lead to a more stable axis rotation.

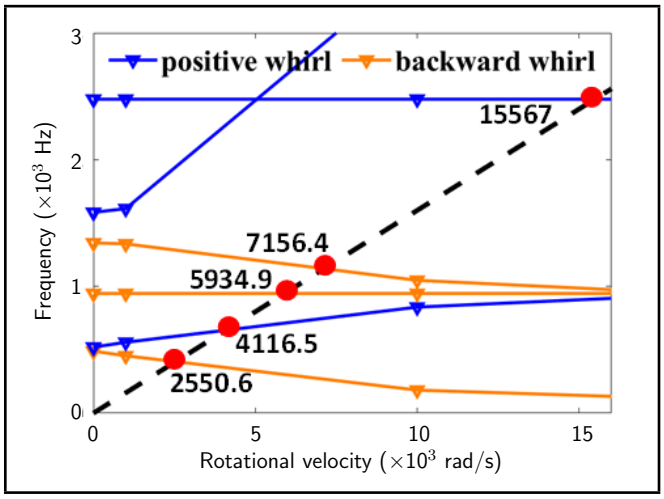

Figure 11. Campbell diagram of the rotor system from the proposed FE model.

FUNDING

The National Natural Science Foundation of China under Contract No. 52175120, 51975068 and 52211530085.

CONFLICT OF INTEREST

The authors declared that they have no conflicts of interest.

REFERENCES

[1] Pan, G., Song, B.W., Huang, Q.G., Development and key techniques of unmanned undersea system, *Journal of Unmanned Undersea Systems*. **25**(02) (2017) 44–51.

[2] Xie, C., Hao, L.N., Deng, S., A nonlinear system of a high-speed bearing rotor with outer raceway spalls and its vibration response analysis, *Journal of Vibration and Shock*. **41**(04) (2022) 262–269.

[3] Liu, J., An, C., Pan, G., A vibration model of a rotor system with the sinusoidal waviness by using the non-Hertzian solution,

Journal of Multi-body Dynamics. **236**(1) (2022) 151–167.

[4] Hu, J., Yang, D.B., A rotor coupling fault mechanism modeling based on the deformation motion vector analysis method, *Journal of Mechanical Engineering*. **57**(15) (2021) 91–104.

[5] Sun, J.L., Simulation for nonlinear oscillation of an underwater turbine bearing-rotor, *Journal of Computer Measurement and Control*. **20**(3) (2012) 747–750.

[6] Li, C.X., Wang, Y., Duan, H., Effects of rotor parameters on transient process of turbine, *Journal of Unmanned Undersea Systems*. **26**(1) (2018) 78–84.

[7] Song, W., Dynamic properties of torpedo turbine rotor system in three speed-up processes, *Journal of Dynamics and Control*. **14**(3) (2016) 235–240.

[8] Ehrich, F.F., Observations of Nonlinear phenomena in rotordynamics, *Journal of System Design and Dynamics*. **2**(3) (2008) 641–651.

[9] Tiwari, M., Gupta, K., Prakash, O., Effect of radial internal clearance of a ball bearing on the dynamics of a balanced horizontal rotor, *Journal of Sound and Vibration*. **238**(5) 2000 723–756.

[10] Harsha, S.P., Sandeep, K., Prakash, R., The effect of speed of balanced rotor on nonlinear vibrations associated with ball bearings, *International Journal of Mechanical Sciences*. **45**(4) (2003) 725–740.

[11] Li, M., Instability excited by internal damping in flexible rotors supported on rolling bearings, Master thesis, Northwestern Polytechnical University, Xi'an, China, 2013.

[12] Sang, X., Liao, M.F., Wu, F.Y., Experimental study on rotor-dynamic behavior dependent on aero-engine bearing inner ring assembly technologies, *Journal of Propulsion Technology*. **12** (2015) 1874–1880.

[13] Song, W., Yang, C.S., Chen, Z.W., Nonlinear dynamic characteristics analysis of torpedo turbine rotor-rolling bearing system, *Journal of Unmanned Undersea Systems*. **29**(6) (2021) 690–694.

[14] Li, Y.F., Wu, Z.Y., Lu, B.H., Influence of clearance on load distribution of single row four-point contact ball slewing bearings, *Journal of Mechanical Transmission*. **34**(3) (2010) 56–58.

[15] Hu, Q.H., Deng, S.E., Teng, H.F., Optimization of rotor-bearing system with nonlinear dynamics considering internal clearance, *Journal of Aerospace Power*. **9** (2011) 2154–2160.

[16] Meng, S.Y., Liu, F., Li, M.W., Research on vibration characteristics of deep groove ball bearing-rotor system for asynchronous motor, *Journal of Bearing*. **7** (2021) 8–15.

[17] Liu, J., Wu, H., Shao, Y.M., Investigation for vibrations of tapered roller bearing considering the surface waviness on the rib of the inner race, *Journal of Mechanical Engineering*. **54**(8) (2018) 26–34.

[18] Liu, J., Xu, Z.D., A simulation investigation of lubricating characteristics for a cylindrical roller bearing of a high-power gearbox, *Tribol International*. **167** (2022) 107373.

[19] Ding, D.S., Liu, Y.Q., Yang, S.P., Analysis of the influence of outer ring raceway peeling fault on the dynamic response of a rolling bearing, *Journal of Vibration and Shock*. **41**(8) (2022) 141–148.

[20] Liu, J., Wang, L.F., Shi, Z.F., Dynamic modelling of the defect extension and appearance in a cylindrical roller bearing, *Mech. Syst. Signal Process* 2022; **173**(3) 109040.

[21] Hong, J.Z., Jiang, L.Z., Flexible multibody dynamics with coupled rigid and deformation motions, *Journal of Advances in Mechanics*. **1** (2000) 15–20.

[22] Liu, J., Tang, C.K., Dynamic modeling and simulation of a flexible-rotor ball bearing system. *Journal of Vibration and Control* 2021. https://doi.org/10.1177/10775463211034347.

[23] Li, R.Z., Hao, D.X., Simulation on critical rotation speed of high-speed rotor of gas turbine, *Torpedo Technology*. **22** (6) (2014) 457–460.